RESEARCH ARTICLE

Check for updates

Carbonized polymer dots/TiO$_2$ photonic crystal heterostructures with enhanced light harvesting and charge separation for efficient and stable photocatalysis†

Yue Zhao,‡ Qingsen Zeng,‡ Tanglue Feng, Chunlei Xia, Chongming Liu, Fan Yang, Kai Zhang [ID] and Bai Yang [ID] *

TiO$_2$ photonic crystals (PCs) are widely interesting in photocatalysis due to their slow photon effect for efficient light harvesting. However, their performance is limited by the narrow absorption range and fast charge recombination. In this work, an efficient strategy is developed to enhance the light harvesting and charge lifetime through fabricating TiO$_2$ PC/carbonized polymer dot (CPD) heterostructures. The CPDs with a band gap of 2.08 eV are used to broaden the light absorption range. The energy level of CPDs matches well with TiO$_2$ PCs, forming a type-II heterojunction. The staggered energy levels of CPD/TiO$_2$ PC heterostructures are helpful for charge separation and thus suppressed charge recombination, which is demonstrated by the transient photovoltage (TPV) measurements. Therefore, the CPD/TiO$_2$ PC heterostructures exhibit obviously better photocatalytic performance than individual TiO$_2$ PCs. The combination of CPDs and inorganic semiconductors provides a variety of possibilities for the further development of high-efficiency photocatalysts.

1. Introduction

During the last few decades, environment issues and water pollution have become increasingly serious, which has stimulated scientific research into green, efficient and low-cost photocatalysts, such as metal oxides (TiO$_2$, ZnO, SnO$_2$, ZrO$_2$)[1–6] and semiconductor quantum dots (ZnS).[7] Among them, TiO$_2$ is one of the most significant photocatalysis materials owing to its excellent stability, low toxicity and low cost.[8–12] Many strategies have been adopted to promote the photocatalytic performance, including doping heteroatoms,[13] loading co-catalysts,[14] and preparing composites with other semiconductors.[9,11] However, the utilization efficiency of sunlight of TiO$_2$ is less efficient due to the large bandgap (3.0–3.2 eV).[15] Besides, the rapid charge recombination rate primarily limits the photocatalytic performance.[16,17] Therefore, strategies for synergetic enhancement of light harvesting and charge lifetime are of great significance to improve photocatalytic efficiency.

Photonic crystals (PCs) possess a photonic stop band (PSB) and thus can slow down the photons near the PSB edges, which

State Key Laboratory of Supramolecular Structure and Materials, College of Chemistry, Jilin University, Changchun, 130012, P. R. China. E-mail: byangchem@jlu.edu.cn

† Electronic supplementary information (ESI) available. See DOI: 10.1039/c9qm00556k
‡ Yue Zhao and Qingsen Zeng contributed equally to this work.

offers a unique way to promote light harvesting,[12,18–20] and have attracted much interest in photocatalysis.[21–23] The periodic dielectric structure endows PCs with a unique structure and optical properties, such as large specific surface area with a uniform macroporous structure, and controlling and manipulating incident light with high absorption efficiency. Not only can the PCs be assembled with a conductive substrate to fabricate photoelectrodes for photoelectrocatalysis,[24,25] but their powders are able to be prepared on a large scale *via* substrate-free procedures for photocatalysis.[12,22] TiO$_2$ PCs have shown higher photocatalytic activity compared to TiO$_2$ nanocrystals as a result of the slow photon effect, which plays a key role in the enhancement of the photocatalytic performances for TiO$_2$ PCs.[26] In spite of the improved photocatalytic properties for TiO$_2$ PCs, the absorption edge still locates at the ultraviolet region and the limited charge lifetime in individual TiO$_2$ PCs restricts the further improvement of photocatalytic performance. Until now, few studies have reported a method to simultaneously achieve enhanced light harvesting and prolonged charge lifetimes in TiO$_2$ PCs (Table S1, ESI†). Therefore, it's urgent to develop new efficient strategies to enhance the light harvesting and charge separation of TiO$_2$ PCs to further improve the photocatalytic efficiency.[12]

Carbonized polymer dots (CPDs), as a new and significant member of the carbon-based nanomaterials family, have caused increasing interest in recent years,[27,28] and are widely

This journal is © The Royal Society of Chemistry and the Chinese Chemical Society 2019

Mater. Chem. Front., 2019, **3**, 2659–2667 | 2659

applied in bioimaging,[29] photoelectronic devices,[30] anti-counterfeiting,[31] photocatalysis,[32] photothermal therapy[33,34] and sensing,[35] due to their superior light absorption, color-tunable photoluminescence, excellent electron transfer ability, great photo-chemical stability and low toxicity. CPDs are usually prepared through the procedure of hydrothermal condensation crosslinking and carbonization (HCCC) from small molecules and/or polymers, which contain multiple polar carboxyl, amino or hydroxyl groups.[36] Very recently, a new strategy of hydrothermal addition polymerization and carbonization (HAPC) was developed by our group to prepare CPDs with ultrahigh yields (ca. 85%).[37] Rich surface polar groups of CPDs make them easily anchor with other semiconductor materials. Besides, CPDs have a wide light absorption range and can generate e^-/h^+ pairs efficiently under light irradiation. Fast charge separation and transfer have been observed in CPD-based hybrid materials.[38,39] Accordingly, CPDs have been successfully used in efficient solar cells,[30] photocatalysis,[40–42] and photoelectrocatalysis[43] through coupling with semiconductors. Therefore, it is expected that the light-harvesting ability and charge separation/transfer dynamics of TiO_2 PCs can be improved with CPDs to fabricate high-efficiency composite photocatalysts.

In this work, an efficient method that enhances the light harvesting and charge separation of TiO_2 PCs is developed through fabricating CPD/TiO_2 PC heterostructures. The CPD/TiO_2 PC heterostructures exhibit obviously improved photocatalytic performance compared to pure TiO_2 PCs. The essential mechanisms of the promoted performance are investigated and discussed in detail. On the one hand, the CPD/TiO_2 PC heterostructures have much broader light absorption range than TiO_2 PCs because of the narrow bandgap of CPDs. On the other hand, the energy level of CPDs matches well with TiO_2 PCs, and type-II heterojunctions are formed between the CPDs and TiO_2 PCs. The staggered energy levels of CPD/TiO_2 PC heterostructures are helpful for charge separation and thus suppressed charge recombination, which is demonstrated by the transient photovoltage (TPV), transient photocurrent and electrochemical impendence spectra (EIS) measurements.

2. Experimental methods

2.1 Materials

Styrene monomer (99%), methylene blue and anhydrous citric acid (98%) were purchased from Aladdin. p-Aminosalicylic acid (99%) was obtained from J&K Scientific Ltd. Methanol, concentrated hydrochloric acid (HCl, AR) and sodium hydroxide (NaOH, AR) were purchased from Beijing Chemical Works. Tetrabutyl titanate (TBT) was obtained from Guangfu Chemical Reagent. All chemicals were used as received.

2.2 Preparation of CPDs

The CPDs with narrow band gaps were synthesized according to the modified method of previous work.[27] Citric acid (CA) (1 mmol) and p-aminosalicylic acid (1 mmol) were dissolved in 10 mL of water, and the pH was adjusted by concentrated

hydrochloric acid to ~1. The mixture was heated at 200 °C for 8 h in a poly(tetrafluoroethylene) (Teflon)-lined autoclave. After cooling down, the as-prepared solution was filtered using a 0.22 μm filter to remove the large particles, and then immediately dialyzed in deionized water through a dialysis bag with a molecular weight cut-off of 3500 for 24 h, during which the deionized water was changed every 3–4 h to fully remove the excess precursors and byproducts. Finally, a clear brown solution was achieved, and a red brown CPD powder was obtained after removing the water though freeze-drying.
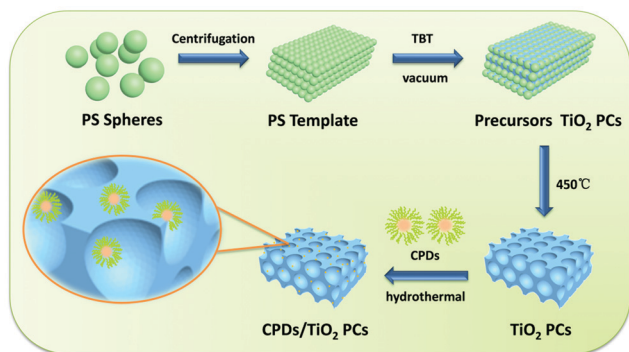
2.3 Preparation of TiO_2 PCs

The polystyrene (PS) microspheres were prepared according to the method in previous work.[12] The styrene monomer was washed with NaOH solution (0.1 M) and deionized water to remove the 4-tert-butylcatechol stabilizer. The monodispersed PS dispersion with a diameter of 265 nm was synthesized by emulsifier-free emulsion polymerization with potassium peroxydisulfate as an initiator. The PS dispersion was centrifuged at 3000 rpm for 18 h to prepare the PS colloidal crystal templates. The TiO_2 precursors (TBT) permeated the voids in the close packed PS colloidal crystal templates through a forced impregnation method.[44] In a typical procedure, the PS template was soaked in methanol for 30 min. After pouring off the methanol, the TBT was added into the PS templates, and then the vessel was kept in a vacuum overnight to make the TBT permeate the voids. The excess TBT was poured away, and the solid block was dried at room temperature followed by annealing in the tubular furnace at 450 °C for 12 h to remove the PS microspheres. Finally, the white TiO_2 PCs with a well periodic macroporous structure were obtained.

2.4 Preparation of CPD/TiO_2 PC heterostructures

The CPD/TiO_2 PC heterostructures were prepared using a hydrothermal method. In a typical procedure (as described in Scheme 1), 50 mg of TiO_2 PCs with different ratios of CPDs were added into the mixed solution of 5 mL of water and 1.5 mL of alcohol. To adequately combine the TiO_2 PCs with CPDs, the mixture was transferred into a 25 mL poly(tetrafluoroethylene) (Teflon)-lined autoclave and kept stirring for 4 h before this suspension was heated at 140 °C for 4 h. After cooling down to room temperature naturally, the resulting composites of CPD/TiO_2 PC heterostructures were collected through centrifugation and then washed with deionized water three times. Finally, light grey powders of CPDs/TiO_2 PCs were obtained after drying.

2.5 Photocatalytic activity and stability measurements

Visible light photocatalytic experiments of Methylene Blue (MB) degradation were carried out to detect the catalytic activity of the CPD/TiO_2 PC heterostructures. 20 mg of photocatalyst (CPDs, CPDs/TiO_2 PCs heterostructures, TiO_2 PCs) was put into 20 mL of MB aqueous solution (20 mg L^{-1}), and the mixture was stirred for 30 min in the dark to reach the adsorption–desorption equilibrium between the dye and catalyst. Next, the solution was cooled with a condensing circulation system and

Scheme 1 Schematic procedures for the preparation of CPD/TiO$_2$ PC heterostructures. In the magnified scheme of CPD/TiO$_2$ PC heterostructures, the size of the CPDs is enlarged to make them visible.

irradiated with a Xe arc lamp fitted with a UV cutoff filter ($\lambda > 420$ nm), whose light intensity was set to 100 mW cm^{-2} (AM1.5 conditions) with the aid of a calibrated Si reference solar cell. During the irradiation, 1 mL of reaction solution was removed at regular intervals, and the change of the MB concentration was analyzed with a ultraviolet-visible spectrophotometer. The stability measurement was performed for 6 repeated cycles under visible ($\lambda > 420$ nm, former 3 cycles) and full-spectrum (latter 3 cycles) simulated sunlight radiation. The CPD/TiO$_2$ PC heterostructure photocatalysts were recycled, and carefully collected through centrifugation after each single degradation experiment.

2.6 Transient photovoltage (TPV) characterization

The sample chamber consisted of a platinum wire gauze electrode (with the transparency of *ca.* 50%) as a top electrode, a mica spacer with a thickness of 10 mm as an electron isolator, and a glass substrate covered with indium-tin oxide (ITO) as a bottom electrode. The samples were sandwiched between the electron isolator and bottom electrode, and excited with a laser pulse (365 nm with pulse width of 5 ns) generated by a third harmonic Nd:YAG laser (Polaris, New Wave Research, Inc.). The intensity of the pulse was adjusted with a neutral gray filter and measured by an EM500 single-channel joulemeter (Molectron, Inc.). The TPV data were obtained through a 500 MHz digital phosphor oscilloscope (TDS 5054, Tektronix) with a preamplifier.

2.7 Characterization

A shimadzu 3600 UV-visible-NIR spectrophotometer was used to measure the UV-visible absorption spectra. The PL spectra were collected by a Shimadzu RF-5301 PC spectrometer. Fourier transfer infrared (FT-IR) measurements were obtained from a Nicolet AVATAR 360 FT-IR spectrophotometer. Scanning electron microscope (SEM) images were taken using a HITACHI SU800 at 3 kV 10 mA. The morphologies of the PS, TiO$_2$ PCs and CPD/TiO$_2$ PC heterostructures on the super thin carbon film were observed by transmission electron microscopy (TEM), which was performed with a JEM-2100F microscope operated at 200 kV using a CCD camera. XPS spectroscopy was investigated by an ESCA LAB 250. The crystallinity and phase of the

TiO$_2$ PCs was studied by XRD using a Empyrean Diffractometer with Cu Kα radiation at 40 kV and 40 mA. The electrochemical impedance (EIS) spectra and transient photocurrent density curves were both collected by a CHI 660E electrochemical workstation in 0.1 M KOH aqueous solution. The transient photocurrent density curves were measured at 1 V (SCE), and the ESI spectra were collected under illumination. Ultraviolet photoelectron spectra (UPS) were collected by a spectrometer (PREVAC sp.z.0.0, R3000).

3. Results and discussion

3.1 CPD/TiO$_2$ PC heterostructures

The procedures of preparing CPD/TiO$_2$ PC heterostructures are exhibited in Scheme 1. In this work, the TiO$_2$ PCs are prepared through substrate-free procedures, which can be easily used to enlarge production. First, through centrifuging the polystyrene (PS) solution microspheres, we obtain the close-packed colloidal crystal templates. Subsequently, TiO$_2$ precursors (TBT) permeate the voids in the close packed PS colloidal crystal templates using a forced impregnation method. Third, TiO$_2$ PCs with a three-dimensionally ordered macroporous structure are achieved *via* a high-temperature annealing process, and the templates are removed completely at the same time. Finally, the CPDs are introduced into TiO$_2$ PCs to form CPD/TiO$_2$ PC heterostructures through a mild hydrothermal process.

Herein, PS microspheres with diameters $\sim$265 nm are used as polymer templates to prepare TiO$_2$ PCs (Fig. S1, ESI†). Fig. 1a shows an SEM image of the close-packed PS microsphere colloidal crystal templates, and they present a highly ordered and face-centered cubic arrangement. Through the processes of precursor infiltration under vacuum, followed by template removal at high temperature, we successfully synthesize the TiO$_2$ PCs with a three-dimensionally ordered macroporous structure. Fig. 1b shows the SEM images of TiO$_2$ PCs. We observe the ordered array of the macropore structure with periodically uniform distribution of macroporous size ($\sim$176 nm). According to the modified Bragg's law:[12,45]

$$\lambda = 2\sqrt{\frac{2}{3}}D\sqrt{n_{\text{TiO}_2}{}^2 f + n_{\text{void}}{}^2(1-f) - \sin^2\theta}$$

where λ is the wavelength related to the PGB, D is the macropore size, n is the refractive index, f is the volume percentage of TiO$_2$ (regularly 0.26), and θ is the light incident angle. When the incident angle θ equals 0, the PGB position of TiO$_2$ PCs only depends on the macropore size, and is calculated to be 376 nm based on the above equation. Therefore, the PSB of this periodic TiO$_2$ PC locates at the absorption edge region of anatase TiO$_2$. In general, the photons near the PSB edge can be slowed down to promote light absorption. This phenomenon is called the slow photon effect, which increases the photon-to-electron conversion efficiency at the absorption edge region, thus resulting in outstanding photocatalytic performance.[12] Fig. S2 (ESI†) shows the optical image of the PC powders. Because of the angle-dependent structural colors of the PC materials, the origin of the iridescent colors is clearly observed. This three-dimensionally ordered
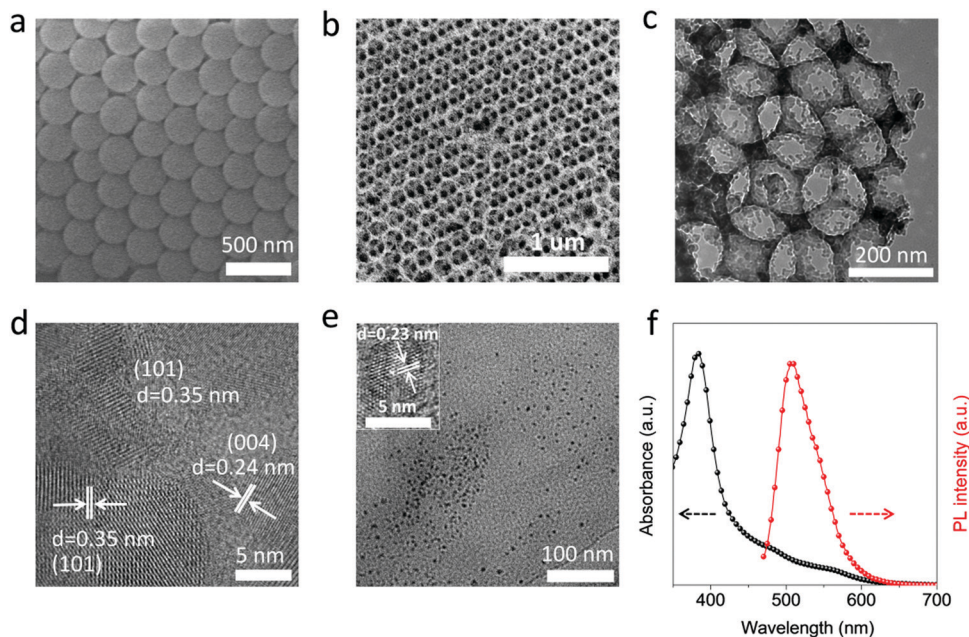
This journal is © The Royal Society of Chemistry and the Chinese Chemical Society 2019

Mater. Chem. Front., 2019, **3**, 2659–2667 | **2661**

Fig. 1 Characterization of TiO_2 PCs and CPDs prepared from *p*-aminosalicylic acid and citric acid precursors. (a) SEM image of closed-packed PS microspheres. (b) SEM, (c) TEM and (d) HR-TEM images of the as-prepared TiO_2 PCs. (e) TEM image of the CPDs. Inset shows the HR-TEM image of the CPDs. (f) UV-visible absorption and steady-state photoluminescence spectra of the CPDs.

macroporous structure can be also observed in the TEM image (Fig. 1c). As shown in Fig. 1d, the HR-TEM image reveals that the skeleton structures of PCs are made up by polycrystalline TiO_2 nanoparticles, which have good crystallinity and present obvious diffraction fringes. The lattice distances of 0.35 nm and 0.24 nm correspond to (101) and (004) facets of anatase TiO_2, respectively. Furthermore, X-ray diffraction (XRD) patterns suggest that the crystal phase of TiO_2 PCs is anatase (Fig. S3, ESI†), which is in good agreement with the results of HR-TEM images. According to previous reports, anatase TiO_2 has an indirect bandgap, and thus possesses much longer carrier lifetime compared to rutile TiO_2 with a direct bandgap. This is propitious to achieve a high-performance photocatalyst based on the anatase TiO_2 PCs.

To further improve the light absorption of anatase TiO_2 PCs (3.2 eV), the CPDs with narrow band gap are incorporated into TiO_2 PCs to fabricate composite materials. The CPDs with strong visible absorption were synthesized according to previous work.[27] Typically, citric acid and *p*-aminosalicylic acid are selected as the precursors, and the CPDs are prepared under a more acidic hydrothermal environment (pH = 1.0) to increase the carbonization degree, and thus to enhance and broaden the absorption. The TEM image of the CPDs is presented in Fig. 1e, and the CPDs show quasi-spherical shape with the average size of 4.9 nm. The HR-TEM image reveals that the CPDs are crystalline with a lattice spacing of 0.23 nm (inset of Fig. 1e). As shown in Fig. 1f, the UV-vis spectrum of CPDs gives two absorption peaks located at 382 and 507 nm. The CPDs show strong and broad visible absorption, and a band gap of 2.08 eV is calculated from the absorption spectrum (Fig. S4, ESI†). The narrow band gap and strong light

absorption of the CPDs are helpful to improve the light harvesting of TiO_2 PCs and thus photocatalytic performance. A strong fluorescence-emission peak at 507 nm with negligible excitation-dependent properties is observed in the photoluminescence spectrum (Fig. 1f and Fig. S5, ESI†).[27]

The CPD/TiO_2 PC composite photocatalysts were constructed using a mild hydrothermal method. In the Fourier transform infrared (FT-IR) spectrum of the CPDs (Fig. 2a), the broad peak around 3200 cm^{-1} belongs to the characteristic absorption of amino, carboxyl and hydroxyl groups, indicating that the CPDs inherit a large amount of polar groups of the precursors (citric acid and *p*-aminosalicylic acid). These surface polar groups make CPDs easily dissolve in water, and also act as a bridge to link CPDs and TiO_2 PCs at the same time. Functional groups of amino and carboxyl can high-effectively bond with TiO_2 through coordinating with Ti^{4+}.[46] From the FT-IR spectrum of CPD/TiO_2 PC composites (Fig. 2a), many characteristic absorption peaks of CPDs appear in the FT-IR spectrum of CPD/TiO_2 PC heterostructures. The peaks located at 3425, 1631, 1385 and 1154 cm^{-1} are attributed to the vibrations of polar groups (amino, carboxyl or hydroxyl), C=N/C=C, C–O (phenoxy) and C–O, respectively. Besides, no similar absorption peaks are observed in the FT-IR spectrum of individual TiO_2 PCs. Thus, it is suggested that CPDs are successfully introduced into TiO_2 PCs.

SEM and TEM images demonstrate that the CPD/TiO_2 PC heterostructures maintain an intact three-dimensionally ordered macroporous structure after hydrothermal and multistep centrifugal purification procedures (Fig. 2b and c). The good structural stability of CPD/TiO_2 PC heterostructures is propitious to the durability of photocatalytic performance. HR-TEM measurement was further carried out to study the distinct structure of the
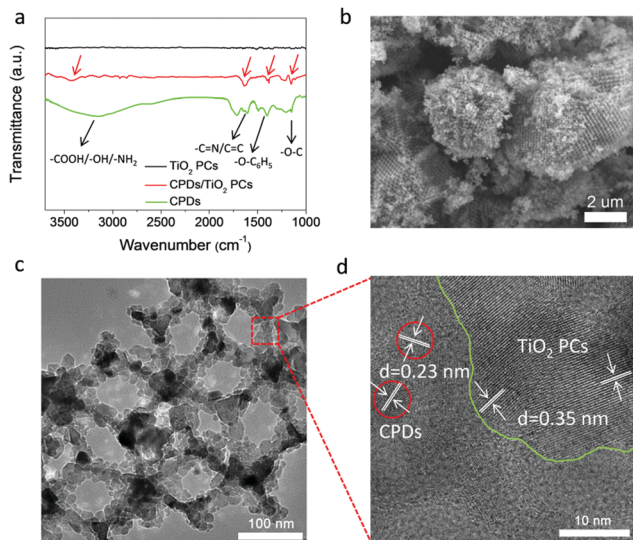
2662 | *Mater. Chem. Front.*, 2019, **3**, 2659–2667

This journal is © The Royal Society of Chemistry and the Chinese Chemical Society 2019

Fig. 2 Characterization of a CPD/TiO$_2$ PC heterojunction. (a) FT-IR spectra of CPDs, TiO$_2$ PCs and CPD/TiO$_2$ heterostructures. (b) SEM, (c) TEM and (d) HR-TEM images of CPD/TiO$_2$ PC heterostructures.

CPD/TiO$_2$ PC heterostructures. As shown in Fig. 2d, the crystal fringes of CPDs and TiO$_2$ are both observed, which further indicates that CPDs are anchored on the surface of the TiO$_2$ PCs. Due to the high contrast and crystallinity of TiO$_2$ nanoparticles, their lattice fringes are clearer and more obvious than that of CPDs. Based on the above characterization, it is concluded that CPD/TiO$_2$ PC heterostructures are successfully constructed.

3.2 Photocatalytic performance

In this part, the photocatalytic performance of the CPD/TiO$_2$ PC heterostructures is investigated in detail. Fig. 3a and b present the photocatalytic degradation of methylene blue (MB) and their kinetics in different catalysts under visible light irradiation ($\lambda > 420$ nm). The concentration of MB is recorded by UV-visible absorption spectra, and the variation of concentration ratio (final to initial concentration, C/C_0) with irradiation time is exhibited in Fig. 3a. MB is slowly degraded and decomposed by about 20% with no catalysts after 120 min irradiation, while sole CPDs show negligible photocatalytic performance of MB degradation (25%). Once TiO$_2$ PC catalysts are adopted, the degradation of MB is promoted to 59%. Furthermore, when the CPDs are introduced into the TiO$_2$ PCs to fabricate a CPD/TiO$_2$ PC heterostructure photocatalyst, the best photocatalytic activity is achieved with enhanced degradation efficiency of up to 85%, indicating that CPDs play a critical role in the improved performance of CPD/TiO$_2$ PC heterostructures. The degradation rate constants of MB for different photocatalysts are studied. It is noted that the kinetics of the degradation process follow a pseudo first order reaction, which can be expressed by the equation: $\ln(C/C_0) = -k_{app}t$, where k_{app} is the apparent reaction rate constant and t is the time.[1] The k_{app} can be obtained from the slope of linear plots. As shown in Fig. 3b, the k_{app} for CPDs is 0.209×10^{-2} min^{-1}, while that of TiO$_2$ PCs and CPD/TiO$_2$ PC heterostructures is 0.713×10^{-2} min^{-1} and 1.529×10^{-2} min^{-1}, respectively. The CPD/TiO$_2$ PC heterostructures present an over 2-fold increase of
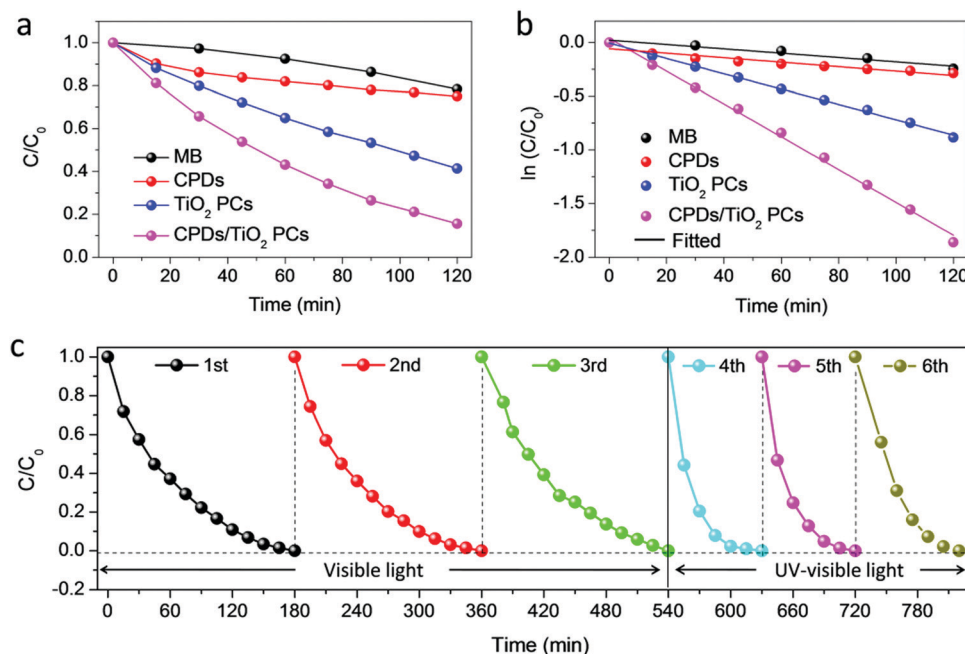

Fig. 3 Photocatalytic activity and stability of CPD/TiO$_2$ PC heterostructures for the degradation of MB. (a) Evolution of relative concentration (C/C_0) of MB in different photocatalysts under one-sun visible light irradiation ($\lambda > 420$ nm). The intensity of the lamp is set to 100 mW cm^{-2} (AM1.5 conditions) with the aid of a calibrated Si reference solar cell. 20 mg of photocatalyst are used. (b) ln(C/C_0) as a function of time. (c) 6 continuous repeated cycles are carried out to test the stability of the CPD/TiO$_2$ PC heterostructure photocatalysts under visible ($\lambda > 420$ nm, former 3 cycles) and full-spectrum (latter 3 cycles) simulated sunlight radiation.

This journal is © The Royal Society of Chemistry and the Chinese Chemical Society 2019

Mater. Chem. Front., 2019, **3**, 2659–2667 | **2663**

degradation rate compared to the individual TiO$_2$ PCs. The mechanisms of enhanced performance are systematically studied in the next part. Besides, the effects of CPD content on photocatalytic performance are investigated. When the content of CPDs reaches 0.5wt%, the CPD/TiO$_2$ PC heterostructures exhibit the best catalytic activity (Fig. S6, ESI†).

The stability and reusability of the CPD/TiO$_2$ PC heterostructures are also studied. As shown in Fig. 3c, 6 continuous repeated cycles are carried out to test the stability of the CPD/TiO$_2$ PC for photocatalytic degradation. The former 3 cycles are performed under visible ($\lambda > 420$ nm) simulated sunlight. It is observed that the MB is all degraded within 180 min, and the stability of the CPD/TiO$_2$ PC heterostructures is quite good after 3 recycling photocatalytic experiments. To investigate the stability of the composite photocatalyst in a more real situation, another 3 repeated cycles are conducted under full-spectrum simulated sunlight radiation, where the UV cutoff filter is removed. As presented in Fig. 3c, once the energy of UV-light is introduced, the photocatalytic reaction rate is accelerated obviously and the MB is degraded entirely in less than 90 min. Importantly, the CPD/TiO$_2$ PC heterostructures also maintain excellent stability under complete simulated sunlight radiation.

3.3 Mechanisms of enhanced performance

It is noted that the CPD/TiO$_2$ PC heterostructures exhibit improved photocatalytic efficiency compared with sole TiO$_2$ PCs. The inner synergistic effects between CPDs and TiO$_2$ PCs are explored in detail in this part. Light harvesting is of great importance for a photocatalyst. Fig. 4a presents the absorption spectra of CPDs, TiO$_2$ PCs and CPD/TiO$_2$ heterostructure powders. The TiO$_2$ PCs have strong absorbance in the UV-region ($\lambda < 400$ nm), while their absorbance in visible-light-region ($\lambda > 400$ nm) is negligible. Nevertheless, once CPDs are introduced, the absorption of both UV and visible light is promoted for CPD/TiO$_2$ heterostructures, which is attributed to the wide absorption range of CPDs. As directly observed in the insets of Fig. 4a, the individual TiO$_2$ PCs are pure white, while their color becomes light grey after introducing CPDs, which indicates enhanced light harvesting for CPD/TiO$_2$ heterostructures. The promoted absorbance of CPD/TiO$_2$ heterostructures is beneficial for a photocatalytic reaction.

Besides light harvesting, charge separation is another important factor that affects photocatalytic performance. Charge transfer depends on the energy level alignment between CPDs and TiO$_2$ PCs. Ultraviolet photoelectron spectroscopy (UPS) measurement was used to characterize the energy levels of CPDs. The highest occupied molecular orbital (HOMO) of CPDs is calculated to be -5.32 eV from the UPS spectrum (Fig. 4b). The band gap of CPDs is 2.08 eV, so the lowest unoccupied molecular orbital (LUMO) is determined to be -3.24 eV. The valence band (VB) and conduction band (CB) of anatase TiO$_2$ are -7.40 and -4.20 eV, respectively.[15] Therefore, staggered energy levels are established between CPDs and anatase TiO$_2$ PCs. This indicates that CPD/TiO$_2$ PC heterojunctions belong to type-II heterojunctions, which are beneficial for charge separation and thus suppressed charge recombination. Photogenerated electrons in CPDs can transfer into TiO$_2$ PCs,

while CPDs can accept the holes of TiO$_2$ PCs. To investigate the charge separation dynamics and carrier lifetime, transient photovoltage (TPV) measurements at 355 nm excitation are performed.[47,48] For the TPV response, a positive signal suggests that holes accumulate at the surface of a light-irradiated top electrode. In contrast, a negative signal implies electrons accumulating at the surface of a top electrode.[49–51] As shown in Fig. 4c, both of the TiO$_2$ PCs and CPD/TiO$_2$ PC heterostructures present positive signals, which indicates that photogenerated holes are gathered at the top surface. Compared with sole TiO$_2$ PCs, the CPD/TiO$_2$ PC heterostructures exhibit enhanced TPV response, implying promoted charge separation inside the CPD/TiO$_2$ PC heterostructures. This originates from the increased harvesting of incident light and matched energy level alignment of CPD/TiO$_2$ PC heterostructures. The TPV measurement of individual CPDs was also conducted (Fig. S7, ESI†). A very weak and negative TPV response is observed, which demonstrates that, compared with TiO$_2$ PCs and CPD/TiO$_2$ PC heterostructures, charge separation is weak and photogenerated holes and electrons transfer through the opposite direction inside sole CPDs. This further proves that the enhanced TPV response of CPD/TiO$_2$ PC heterostructures is attributed to the synergic actions between TiO$_2$ PCs and CPDs. Plots of normalized TPV intensity *versus* linear time are presented in Fig. 4d to directly observe the recombination lifetime of photogenerated carriers. In comparison with a half-lifetime of 0.636 ms in TiO$_2$ PCs, the half-lifetime of CPDs/TiO$_2$ PC heterostructures increases to 1.103 ms. The promoted charge lifetime is ascribed to the enhanced charge separation and suppressed charge recombination inside CPD/TiO$_2$ PC heterostructures.

Based on the above discussion, it is concluded that the enhanced light harvesting and charge separation of CPD/TiO$_2$ PC heterostructures accounts for their promoted photocatalytic performance. In order to further investigate the charge generation and separation dynamics in TiO$_2$ PCs and CPD/TiO$_2$ PC heterostructures, the transient photocurrent response and electrochemical impedance spectra (EIS) are measured. As shown in Fig. 4e, the transient photocurrent data are obtained through repeating the on/off illumination cycles at a bias of 1.0 V. The sole TiO$_2$ PCs have a relatively low photocurrent response under each illumination, while CPD/TiO$_2$ PC heterostructures present obviously enhanced reproductive photocurrent response with excellent stability of up to 800 s. This further proves the promoted charge separation in CPD/TiO$_2$ PC heterostructures. Fig. 4f shows the Nyquist plots of TiO$_2$ PCs and CPD/TiO$_2$ PC heterostructures, which are measured under light conditions at a bias of 0 V with a frequency ranging from 0.1 Hz to 200 kHz. Only one circular arc is observed for each sample. In this case, an equivalent circuit containing an electrolyte solution resistance (R_s), interfacial charge-transfer resistance (R_{ct}) and constant phase element (CPE) is used to analyze the charge transfer dynamics of TiO$_2$ PCs and CPD/TiO$_2$ PC heterostructures.[7] Through fitting the Nyquist plots according to the above model, the CPD/TiO$_2$ PC heterostructures have much lower R_{ct} of 26.0 kΩ cm^2 than the sole TiO$_2$ PCs (301 kΩ cm^2), due to the smaller semicircle of CPD/TiO$_2$ PC heterostructures (Table 1). This further proves that the

2664 | *Mater. Chem. Front.*, 2019, **3**, 2659–2667

This journal is © The Royal Society of Chemistry and the Chinese Chemical Society 2019
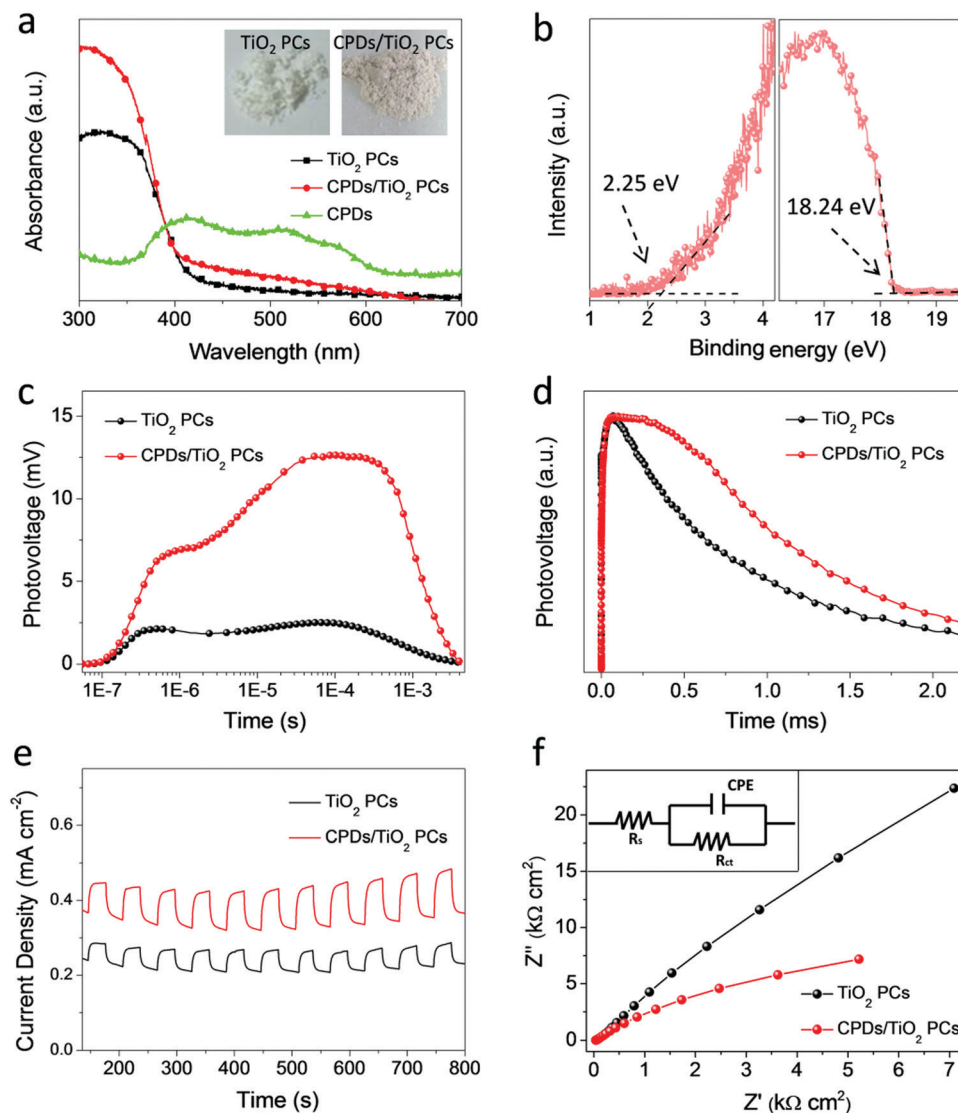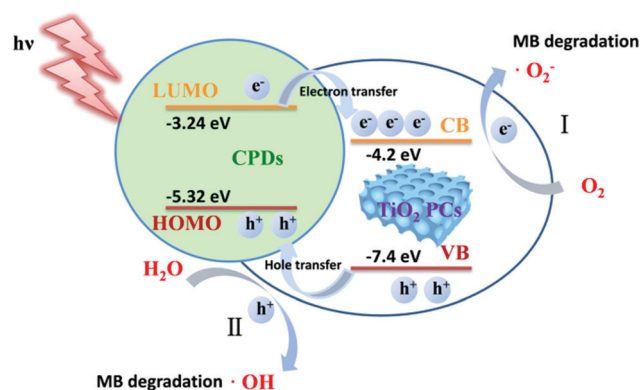
Fig. 4 Photocatalytic mechanisms of CPD/TiO$_2$ PC heterostructures. (a) Absorption spectra of CPDs, TiO$_2$ PCs and CPD/TiO$_2$ heterostructure powders. Insets show the optical photographs of TiO$_2$ PCs (left) and CPD/TiO$_2$ heterostructure (right) powders. (b) Ultraviolet photoelectron spectroscopy (UPS) of CPDs: secondary electron cut-off region (left), magnified spectra near the Fermi edge (right). HOMO = −(21.21 − 18.24 + 2.25) eV = −5.32 eV. (c) Transient photovoltage (TPV) curves of TiO$_2$ PCs and CPD/TiO$_2$ PC heterostructures as a function of exponential time. (d) Plots of normalized transient photovoltage *versus* linear time. (e) Transient photocurrent density, and (f) EIS curves of TiO$_2$ PC and CPD/TiO$_2$ PC heterostructures. The inset in (f) is the equivalent circuit diagram for analyzing charge dynamics.

Table 1 EIS fitting parameters of TiO$_2$ PCs and CPD/TiO$_2$ PC hetero-structures

Samples	R_{ct} (kΩ cm^2)	R_s (Ω cm^2)
TiO$_2$ PCs	301 ± 8	85.6 ± 11.7
CPDs/TiO$_2$ PCs	26.0 ± 0.8	54.5 ± 5.2

incorporation of CPDs accelerates the charge transport and transfer, which is beneficial for the photocatalytic reaction.

According to these control experiments, the photocatalytic MB degradation mechanisms of CPD/TiO$_2$ PC heterojunctions are proposed. As shown in Scheme 2, CPDs are anchored on the TiO$_2$ PCs to form CPD/TiO$_2$ PC type-II heterojunctions with staggered energy level alignment. Therefore, during the

Scheme 2 Schematic photocatalytic mechanisms of CPD/TiO$_2$ PC heterostructures.

This journal is © The Royal Society of Chemistry and the Chinese Chemical Society 2019

Mater. Chem. Front., 2019, **3**, 2659–2667 | **2665**

photocatalytic process, CPD/TiO$_2$ PC heterostructures absorb incident light and produce photogenerated charge carriers. Driven by the staggered energy level alignment, the photogenerated electrons in CPDs transfer rapidly to TiO$_2$ PCs, while the holes in TiO$_2$ PCs are partly extracted by CPDs as a result of the relatively low content of CPDs in the heterostructures. Compared to individual TiO$_2$ PCs, the charge carriers in CPD/TiO$_2$ PC heterostructures are separated rapidly and have much longer lifetimes, which contributes to a photocatalytic reaction. Based on the reported catalytic mechanisms in TiO$_2$/carbon nanomaterial composites, the separated holes and electrons react with water (H$_2$O) and oxygen (O$_2$), respectively, to produce active •OH and •O$_2^-$ radicals,[1,52] which are highly energetic to decompose the MB into CO$_2$, water and other inorganic compounds.

4. Conclusions

In summary, we develop an efficient method to enhance the light harvesting and charge separation of TiO$_2$ PCs through fabricating CPD/TiO$_2$ PC heterostructures. The charge separation dynamics and photocatalytic performance-improved mechanisms of CPD/TiO$_2$ PC heterostructures are deeply investigated. CPD/TiO$_2$ PC heterostructures have much broader light absorption range than individual TiO$_2$ PCs due to the narrow band gap of CPDs. Besides, the energy level of CPDs matches well with TiO$_2$ PCs, and thus type-II heterojunctions are formed between CPDs and TiO$_2$ PCs. The staggered energy levels of CPD/TiO$_2$ PC heterostructures are beneficial for charge separation, thus leading to enhanced charge lifetime. Therefore, the CPD/TiO$_2$ PC heterostructures exhibit obviously improved photocatalytic performance compared to the individual TiO$_2$ PCs. This work highlights the importance of a heterojunction structure for preparing high-performance photocatalysts.

Conflicts of interest

There are no conflicts to declare.

Acknowledgements

References

1 G. Rajender, J. Kumar and P. K. Giri, *Appl. Catal., B*, 2018, **224**, 960–972.

2 R. Georgekutty, M. K. Seery and S. C. Pillai, *J. Phys. Chem. C*, 2008, **112**, 13563–13570.

3 H.-l. Xia, H.-s. Zhuang, T. Zhang and D.-c. Xiao, *J. Environ. Sci.*, 2007, **19**, 1141–1145.

4 X. Fu, L. A. Clark, Q. Yang and M. A. Anderson, *Environ. Sci. Technol.*, 1996, **30**, 647–653.

5 X. C. Ma, Y. Dai, L. Yu and B. B. Huang, *Light: Sci. Appl.*, 2016, **5**, e16017.

6 F. Pincella, K. Isozaki and K. Miki, *Light: Sci. Appl.*, 2014, **3**, e133.

7 L. Wang, G. Zhou, Y. Tian, L. Yan, M. Deng, B. Yang, Z. Kang and H. Sun, *Appl. Catal., B*, 2019, **244**, 262–271.

8 S. Sakthivel and H. Kisch, *Angew. Chem., Int. Ed.*, 2003, **42**, 4908–4911.

9 S. Zhuo, M. Shao and S.-T. Lee, *ACS Nano*, 2012, **6**, 1059–1064.

10 X. Yu, J. Liu, Y. Yu, S. Zuo and B. Li, *Carbon*, 2014, **68**, 718–724.

11 D. Pan, J. Jiao, Z. Li, Y. Guo, C. Feng, Y. Liu, L. Wang and M. Wu, *ACS Sustainable Chem. Eng.*, 2015, **3**, 2405–2413.

12 J. Cai, M. Wu, Y. Wang, H. Zhang, M. Meng, Y. Tian, X. Li, J. Zhang, L. Zheng and J. Gong, *Chem*, 2017, **2**, 877–892.

13 J. C. Yu, J. Yu, W. Ho, Z. Jiang and L. Zhang, *Chem. Mater.*, 2002, **14**, 3808–3816.

14 J. Yu, L. Qi and M. Jaroniec, *J. Phys. Chem. C*, 2010, **114**, 13118–13125.

15 Y. Zhao, Q. Zeng, X. Liu, S. Jiao, G. Pang, X. Du, K. Zhang and B. Yang, *J. Mater. Chem. A*, 2016, **4**, 11738–11746.

16 K. Ozawa, S. Yamamoto, R. Yukawa, R.-Y. Liu, N. Terashima, Y. Natsui, H. Kato, K. Mase and I. Matsuda, *J. Phys. Chem. C*, 2018, **122**, 9562–9569.

17 J. C. Calva-Yáñez, M. Solís de la Fuente, M. Ramírez-Vargas and M. E. Rincón, *Materials For Renewable and Sustainable Energy*, 2018, vol. 7, p. 19.

18 P. Zhou, D. Zhou, L. Tao, Y. Zhu, W. Xu, S. Xu, S. Cui, L. Xu and H. Song, *Light: Sci. Appl.*, 2014, **3**, e209.

19 X. Chen, C. Chardin, K. Makles, C. Caër, S. Chua, R. Braive, I. Robert-Philip, T. Briant, P.-F. Cohadon and A. Heidmann, *Light: Sci. Appl.*, 2017, **6**, e16190.

20 N. V. Konopsky, V. E. Alieva, S. Y. Alyatkin, A. A. Melnikov, V. S. Chekalin and M. V. Agranovich, *Light: Sci. Appl.*, 2016, **5**, e16168.

21 J. Du, X. Lai, N. Yang, J. Zhai, D. Kisailus, F. Su, D. Wang and L. Jiang, *ACS Nano*, 2010, **5**, 590–596.

22 F. Sordello, C. Duca, V. Maurino and C. Minero, *Chem. Commun.*, 2011, **47**, 6147–6149.

23 S. Lee, Y. Lee, D. H. Kim and J. H. Moon, *ACS Appl. Mater. Interfaces*, 2013, **5**, 12526–12532.

24 C. Cheng, S. K. Karuturi, L. Liu, J. Liu, H. Li, L. T. Su, A. I. Tok and H. J. Fan, *Small*, 2012, **8**, 37–42.

25 W. Zhang, X. Zhang, Z. Zhang, W. Wang, A. Xie, C. Xiao, H. Zhang and Y. Shen, *J. Electrochem. Soc.*, 2015, **162**, H638–H644.

26 J. I. Chen, E. Loso, N. Ebrahim and G. A. Ozin, *J. Am. Chem. Soc.*, 2008, **130**, 5420–5421.

27 T. Feng, Q. Zeng, S. Lu, X. Yan, J. Liu, S. Tao, M. Yang and B. Yang, *ACS Photonics*, 2017, **5**, 502–510.

28 Y. Song, S. Zhu, J. Shao and B. Yang, *J. Polym. Sci., Part A: Polym. Chem.*, 2017, **55**, 610–615.

29 J. Liu, D. Li, K. Zhang, M. Yang, H. Sun and B. Yang, *Small*, 2018, **14**, e1703919.

30 T. Ji, B. Guo, F. Liu, Q. Zeng, C. Yu, X. Du, G. Jin, T. Feng, S. Zhu, F. Li and B. Yang, *Adv. Mater. Interfaces*, 2018, **5**, 1701519.

31 S. Tao, S. Lu, Y. Geng, S. Zhu, S. A. T. Redfern, Y. Song, T. Feng, W. Xu and B. Yang, *Angew. Chem., Int. Ed.*, 2018, **57**, 2393–2398.

32 M. Han, S. Zhu, S. Lu, Y. Song, T. Feng, S. Tao, J. Liu and B. Yang, *Nano Today*, 2018, **19**, 201–218.

33 X. Bao, Y. Yuan, J. Chen, B. Zhang, D. Li, D. Zhou, P. Jing, G. Xu, Y. Wang, K. Hola, D. Shen, C. Wu, L. Song, C. Liu, R. Zboril and S. Qu, *Light: Sci. Appl.*, 2018, **7**, 91.

34 D. Li, D. Han, S. N. Qu, L. Liu, P. T. Jing, D. Zhou, W. Y. Ji, X. Y. Wang, T. F. Zhang and D. Z. Shen, *Light: Sci. Appl.*, 2016, **5**, e16120.

35 J. Cui, T. Liu, D. Liang, J. Liu, K. Zhang, B. Yang and Y. Ning, *RSC Adv.*, 2017, **7**, 49330–49336.

36 S. Zhu, Q. Meng, L. Wang, J. Zhang, Y. Song, H. Jin, K. Zhang, H. Sun, H. Wang and B. Yang, *Angew. Chem., Int. Ed.*, 2013, **52**, 3953–3957.

37 C. Xia, S. Tao, S. Zhu, Y. Song, T. Feng, Q. Zeng, J. Liu and B. Yang, *Chem. – Eur. J.*, 2018, **24**, 11303–11308.

38 B. C. M. Martindale, G. A. M. Hutton, C. A. Caputo, S. Prantl, R. Godin, J. R. Durrant and E. Reisner, *Angew. Chem., Int. Ed.*, 2017, **56**, 6459–6463.

39 A. Ferrer-Ruiz, T. Scharl, P. Haines, L. Rodriguez-Perez, A. Cadranel, M. A. Herranz, D. M. Guldi and N. Martin, *Angew. Chem., Int. Ed.*, 2018, **57**, 1001–1005.

40 H. Yu, R. Shi, Y. Zhao, G. I. Waterhouse, L. Z. Wu, C. H. Tung and T. Zhang, *Adv. Mater.*, 2016, **28**, 9454–9477.

41 H. Yu, R. Shi, Y. Zhao, G. I. Waterhouse, L. Z. Wu, C. H. Tung and T. Zhang, *Adv. Mater.*, 2016, **28**, 9454–9477.

42 H. Yu, Y. Zhao, C. Zhou, L. Shang, Y. Peng, Y. Cao, L.-Z. Wu, C.-H. Tung and T. Zhang, *J. Mater. Chem. A*, 2014, **2**, 3344–3351.

43 K.-H. Ye, Z. Wang, J. Gu, S. Xiao, Y. Yuan, Y. Zhu, Y. Zhang, W. Mai and S. Yang, *Energy Environ. Sci.*, 2017, **10**, 772–779.

44 X. Chen, Z. Li, J. Ye and Z. Zou, *Chem. Mater.*, 2010, **22**, 3583–3585.

45 J. Xu, B. Yang, M. Wu, Z. Fu, Y. Lv and Y. Zhao, *J. Phys. Chem. C*, 2010, **114**, 15251–15259.

46 J. Wu, Z. Lan, J. Lin, M. Huang, Y. Huang, L. Fan and G. Luo, *Chem. Rev.*, 2015, **115**, 2136–2173.

47 Q. Bu, S. Li, K. Zhang, Y. Lin, D. Wang, X. Zou and T. Xie, *ACS Sustainable Chem. Eng.*, 2019, **7**, 10971–10978.

48 L. Bi, X. Gao, L. Zhang, D. Wang, X. Zou and T. Xie, *ChemSusChem*, 2018, **11**, 276–284.

49 Q. Bu, S. Li, Q. Wu, L. Bi, Y. Lin, D. Wang, X. Zou and T. Xie, *ChemSusChem*, 2018, **11**, 3486–3494.

50 L. Bi, X. Gao, Z. Ma, L. Zhang, D. Wang and T. Xie, *ChemCatChem*, 2017, **9**, 3779–3785.

51 Q. Zeng, Z. Chen, F. Liu, G. Jin, X. Du, T. Ji, Y. Zhao, Y. Yue, H. Wang, D. Meng, T. Xie, H. Zhang and B. Yang, *Sol. RRL*, 2017, **1**, 1600020.

52 A. Qu, H. Xie, X. Xu, Y. Zhang, S. Wen and Y. Cui, *Appl. Surf. Sci.*, 2016, **375**, 230–241.